# Flying Focus: Spatiotemporal Control of the Laser Focus

## Introduction

The controlled coupling of a laser to a plasma has the potential to address grand scientific challenges including reaching the Schwinger limit,[1] developing compact free-electron lasers,[2] extending colliders to TeV energies,[3–5] and generating novel light sources.[6] Currently, many such applications have limited flexibility and poor control over the laser focal volume. In conventional near-diffraction–limited systems, both the minimum focal-spot size ($w_0 \simeq f^{\#}\lambda$) and longitudinal focusing range ($Z_R \simeq f^{\#2}\lambda$) are linked by the ratio of the focal length to twice the beam radius ($f^{\#} = f/2R$). As a result, these systems require large laser spots to extend their focusing range or waveguides[7–11] to maintain small spots over long distances. At low energies, manipulation of the spatial phase overcame this limitation,[12,13] but a long focal range introduced in this way does not possess dynamic properties. Pulse-front tilt was recently used to introduce a time-dependent rotation of the local wavefront in a scheme called "attosecond lighthouse,"[14] but it lacked the long longitudinal focusing range.

"Flying focus" is an advanced focusing scheme, where a chromatic focusing system combined with chirped laser pulses enables a small-diameter laser focus to propagate nearly 100×

its Rayleigh length while decoupling the speed at which the peak intensity propagates from its group velocity. This unprecedented spatiotemporal control over the laser's focal volume allows the laser focus to co- or counter-propagate along its axis at any velocity. Experiments validating the concept measured subluminal ($-0.09c$) to superluminal ($39c$) focal-spot velocities, generating a nearly constant peak intensity over 4.5 mm. The flying focus allows simple, compact systems to exert novel control over laser–plasma interactions and presents opportunities to overcome current fundamental limitations in laser-plasma amplifiers,[15–18] laser-wakefield accelerators,[19–22] photon accelerators,[23] and high-order frequency conversion.[24,25]

Figure 151.1 shows a schematic of the configuration that generates a flying focus. A diffractive lens with a radially varying groove density $G = r / (\lambda_0 f_0)$ is used to produce a chromatic focus, where $f_0$ is the focal length of the system at the central wavelength $\lambda_0$ and $r$ is the distance from the optical axis. With this lens, the longest wavelength ($\lambda_r$) focuses a length $L \simeq f_0(\Delta\lambda/\lambda_0)$ before the shortest wavelength ($\lambda_b = \lambda_r - \Delta\lambda$). By introducing a laser pulse with a temporally varying wavelength, the focus will move at a velocity given by $v(z) = dz/dt$, where $dz$ is the distance between two focused colors spectrally separated



Negative chirp
(blue to red)
$\Delta\lambda = -9.2$ nm

Diffractive lens
$G_R = 60$ lines/mm

$f_0 = 511$ mm

$\lambda_0$

$\lambda_r$

Longitudinal focal shift
($L = 4.5$ mm)

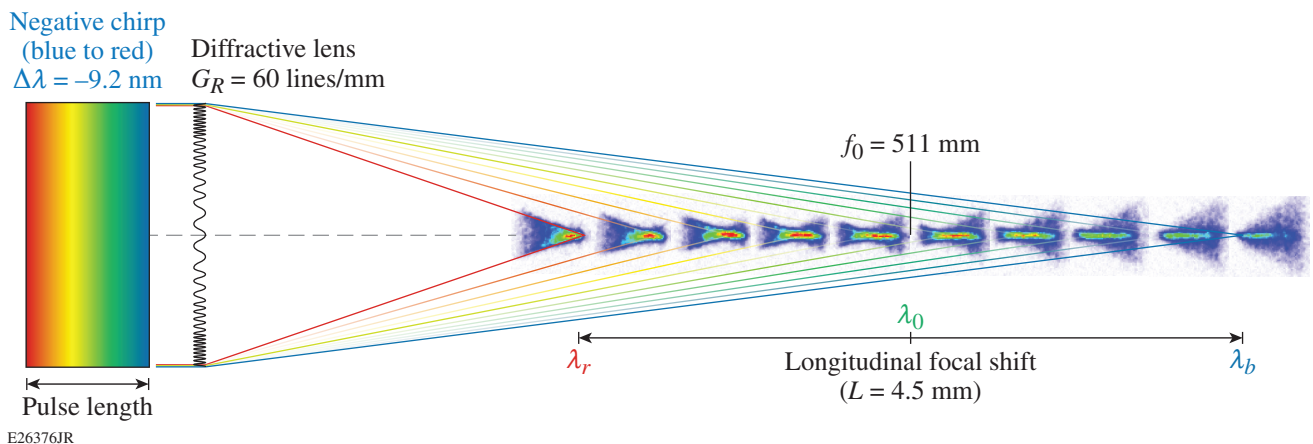$\lambda_b$

Pulse length

E26376JR

**Figure 151.1**
A schematic of the chromatic focusing system coupled to a spectrally chirped laser pulse. Measurements of the temporal evolution of the intensity at various longitudinal locations along the focus are shown. A negatively chirped pulse is shown where the colors change in time from blue to red.

by $\delta\lambda$; $dt = d\tau + dz/c$ is the time it takes for the two colors to reach their respective foci; $d\tau$ is the time between the two colors ($\delta\lambda$) within the chirped laser pulse, and $c$ is the speed of light. By changing the chirp of the laser beam, the time to reach focus for successive colors is varied to provide control of the focal velocity. In general, the velocity of the focus is given by

$$v(z)/c = \left[1 + \left(\frac{d\lambda}{d\tau}\right)^{-1}\left(\frac{dz}{d\lambda}\right)^{-1}c\right]^{-1}, \quad (1)$$

where $dz/d\lambda \simeq -f_0/\lambda_0$ is the longitudinal dispersion provided by the diffractive lens and $\tau = t - z/c$. For a desired longitudinal focal-spot trajectory $z(t)$, a laser chirp can be designed:

$$\lambda(\tau)/\lambda_0 = \left[1 - z(\tau)/f_0\right]^{-1} \approx \frac{z_0(\tau)}{f_0}. \quad (2)$$

For a trajectory with a constant velocity $z(t) = v_0 t$, a linear chirp is required: $\lambda(\tau) = \left(v_0\lambda_0/f_0\right)\tau + \lambda_{r,b}$, where $v_0 = L/T$, $\lambda_{r,b}$ is the initial wavelength, $T$ is the chirped-pulse duration, and $|\tau| < T/2$.

Figure 151.2 shows the velocity of the flying focus [Eq. (1)] for a linearly chirped laser beam ($d\lambda/d\tau = \Delta\lambda/T$). When the wavelengths are arranged in time where the longest wavelength comes first (positive chirp), the focal spot propagates in the forward direction (i.e., away from the diffractive lens) at subliminal velocities. For a negatively chirped laser beam (i.e., when the shortest wavelength comes first), any focal-spot velocity is available. When the pulse duration of the laser is equal to the transit time of the light to propagate across the focal region ($T = L/c$), all of the colors focus simultaneously, generating a long line focus; from Eq. (1) this corresponds to an "infinite" focal velocity.

This article presents experiments that demonstrate the flying focus by measuring the temporal evolution of the focal-spot intensity at various longitudinal locations. From these measurements, the velocity of the focal spot was determined and compared with the theory. The following sections (1) describe the experimental setup where LLE's Multi-Terawatt (MTW) laser[26] was used to demonstrate the flying-focus concept; (2) present the main results where the laser pulse duration was varied to demonstrate unprecedented control of the focal volume; and (3) discuss the potential applications for the flying focus. In particular, we explore using the flying focus to accelerate an ionization wave at the group velocity of accelerating photons,
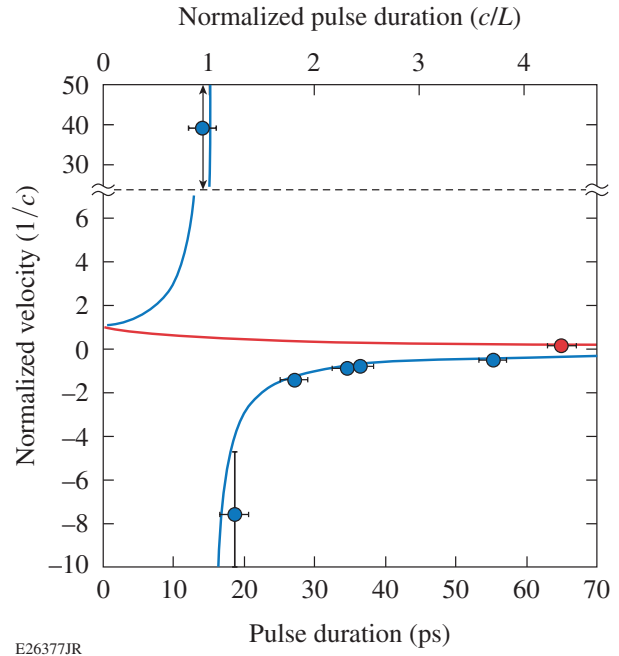


Figure 151.2
The measured (points, bottom axis) and calculated (curves, top axis) [Eq. (1): $v/c = (1 \pm cT/L)^{-1}$] focal-spot velocity plotted as a function of the pulse duration of the laser. The red (blue) symbols represent a positively (negatively) chirped laser pulse. For all but two of the data points, the error in the velocity measurements is smaller than the symbols (<2.5%). For the data point with a pulse duration of 14 ps (very close to the $L/c$), the error in the velocity measurement is large since the focal velocity is nearly 50× the speed of light.

which shows a potential path to generating a deep ultraviolet laser. In the final section, the concept and its potential impact are summarized.
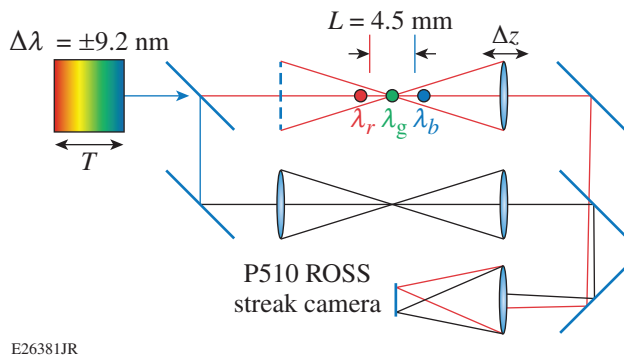
**Experimental Setup**

MTW is a Nd:glass optical parametric chirped-pulse–amplification (OPCPA) laser with a central wavelength of $\lambda_0 = 1054$ nm. The bandwidth ($\Delta\lambda = 9.2$-nm full width at 0.1× maximum) was stretched to produce a 2.6-ns linear chirp, and a set of compressor gratings subsequently compressed the pulse to the desired chirped-pulse duration. Undercompression relative to the transform-limited pulse duration resulted in a positive linear chirp [$\lambda(\tau) = (\Delta\lambda/T)\tau + \lambda_r$] and overcompression resulted in a negative linear chirp [$\lambda(\tau) = -(\Delta\lambda/T)\tau + \lambda_b$]. A diffractive lens with a focal length of $f_0 = 511$ mm (at $\lambda_0$) generated an ~15-$\mu$m-diam focus with a longitudinal separation of $L \simeq 4.5$ mm between the extreme wavelengths. This focal region was nearly 100× the Rayleigh length ($Z_R = 0.05$ mm) of the $f/7$ system.

The velocity of the focus over the longitudinal separation was determined by measuring the radial intensity profile along

the laser beam's axis as a function of time. The experiments used a parallel-path configuration (Fig. 151.3), where the collimated laser beam ($R = 3.5$ cm) was split into two identical beams to form signal and reference paths that were then imaged onto a P510 Rochester optical streak system (ROSS) camera. Inside one of the parallel paths, the signal path was focused by the diffractive lens ($f_0 = 550$ mm) and the reference path was focused by an achromatic lens with an $f_1 = 400$-mm focal length. Both legs used achromatic lenses ($f_{r,s} = 400$ mm) to collimate the light that was then recombined with a slight angle to separate the images at the detector plane. The beams were focused to the detector with a final achromatic lens ($f_2 = 400$ mm) that produced an image of the reference and signal focal regions. Modeling indicated that the optical system was



E26381JR

Figure 151.3
A schematic of the experimental setup. ROSS: Rochester optical streak system.

~3× diffraction limited (~15 $\mu$m) over the wavelength range of interest. The spatial resolution at the detector plane of the ROSS camera was ~50-$\mu$m full width at half maximum (FWHM). The reported pulse duration ($T$) was determined using the reference pulse measured on the ROSS camera. The impulse response of the streak camera was measured to be 7-ps FWHM.

The diameter of the signal pulse as a function of longitudinal position ($z$) along the longitudinal focal length was determined by moving the collection lens ($f_s$) over successive positions spanning slightly beyond the range of extreme focal positions. At each $z$ position, several images were recorded by the streak camera and averaged to increase the signal-to-noise ratio. The reference pulse was used to remove jitter between images. Each composite image generated a measurement of the time between the reference pulse and the signal pulse ($\tau$).

Figure 151.4 shows the results for a negatively chirped laser pulse with a duration of $T = 36.4\pm1$ ps. The images indicate that the focal spot counter-propagated at a velocity of $-0.77c\pm2\%$. When measuring the focal spot at a position closest to the diffractive lens ($z = -1.5$ mm), the diameter of the flying focus was measured to evolve in time from a large spot size to a best-focus spot size over the pulse duration (i.e., the laser spot does not come to focus until the end of the laser pulse). This is in contrast with the measurements that image a position 3.0 mm farther from the diffractive lens ($z = 1.5$ mm). In this case, the focal-spot size was measured to start at its best focus
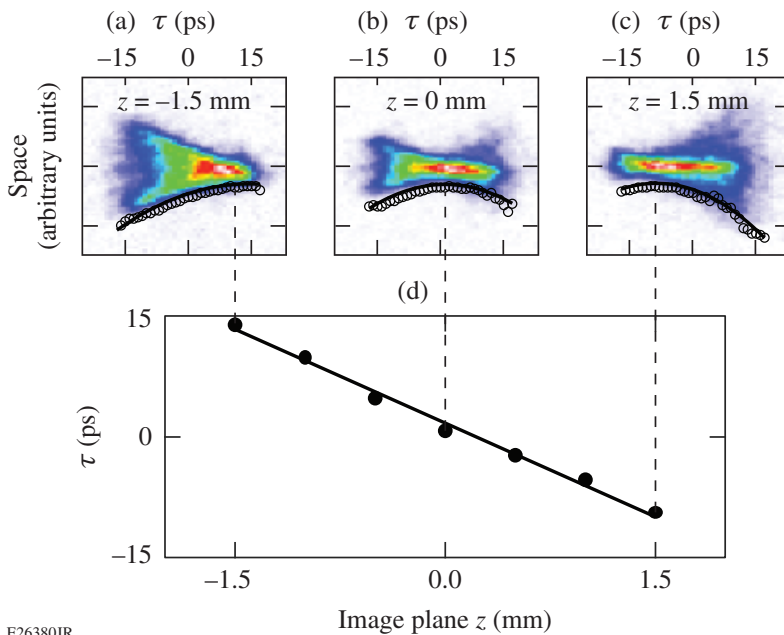


E26380JR

Figure 151.4
Three streak camera images recorded for a pulse duration of $T = 36.4$ ps, where the image plane was focused at (a) $z = -1.5$ mm, (b) $z = 0$ mm, and (c) $z = 1.5$ mm. Plotted over the image is the corresponding full width at 0.2× the peak-power spot size as a function of time. (d) The solid curve is a best fit to the data used to determine the time of minimum spot size ($\tau$). The measured times (points) are shown for this data set. The best-fit line indicates a focal-spot velocity of $v/c = -0.77\pm0.015$.

and expand to a maximum diameter over the duration of the laser pulse (i.e., the laser spot starts at focus and expands until the end of the laser pulse).

The velocity of the focus $\{v = \Delta z/\Delta t = c\,[1 + (\Delta\tau/\Delta z)\,c]^{-1}\}$ was determined by measuring the time of minimum foci ($\tau$) at each image plane ($z$). The slope of a best-fit line to the measured data [Fig. 151.4(b)] was used to determine $m = c\Delta\tau/\Delta z$.

The error in the measurements shown in Fig. 151.2 is given by $\delta v/v = v\delta m$, where $\delta m$ is the uncertainty in each fit.

## Results

Figure 151.5 shows measurements of the flying focus generated by both a negatively and a positively chirped laser pulse. The initial frame of the negatively chirped pulse shows the laser beam entering the focal region, but before it has reached focus.
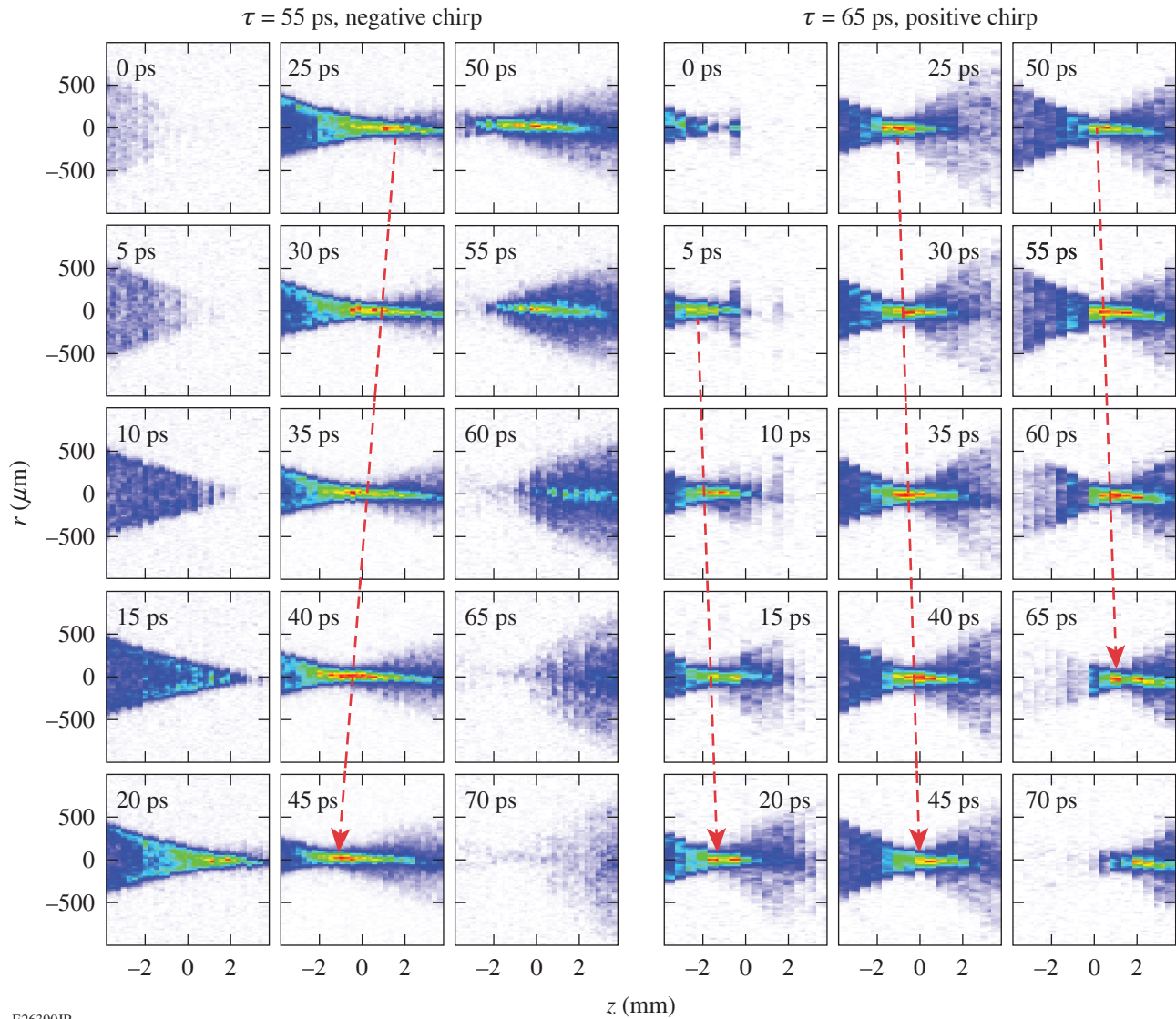


E26390JR

Figure 151.5
The evolution of the flying focus intensity measured for a negative (left) and positive (right) chirped pulse, each with a duration of $T \sim 60$ ps. In each case, the laser is shown propagating into the measurement window (top left) at 0 ps. In the positively chirped case, the laser comes into focus at the left edge of the window ($z \sim -2.5$ mm), in contrast to the negatively chirped case, where the pulse is far from focus. At $t = 25$ ps (top middle), the negatively chirped case shows that the laser has reached focus at the back of the window ($z \sim +2$ mm). Over the next few frames, the focus propagates $\sim -2$ mm in $\sim 20$ ps, corresponding to $-0.3c$, while over the same time, the positively chirped pulse moves forward slowly at $\sim +0.2c$.

Over the next 20 ps, the laser reaches a focus at the far end of the system ($z \sim 2$ mm). This is in contrast with the positively chirped pulse, where the laser comes into focus initially at the front of the measurement window ($z \sim -2$ mm). Comparing the middle row for each data set shows that the focal spots are propagating in opposite directions. For the negatively chirped pulse, the peak intensity moved back toward the lens by $\Delta z \sim 2$ mm over the $\sim 20$ ps corresponding to a velocity of $-0.3c$, while for the positively chirped pulse, the peak intensity moved forward by about the same distance in a comparable time corresponding to a velocity of about $+0.2c$. Figure 151.5 was constructed from temporal measurements of 30 longitudinal locations ranging from $z = -3.75$ mm to $z = +3.75$ mm. The measured images were sliced into temporal bins and recombined given their focal location and measured time ($t$).

The measured velocity of the focus as a function of the pulse duration of the laser compares well with the calculations using Eq. (1) (Fig. 151.2). The results show that when the laser pulse was negatively chirped with a duration of $T = 34.4$ ps, the focal spot counter-propagated at a velocity of $v = -0.87c\pm2\%$. Reducing the pulse duration ($T = 18.6$ ps) resulted in a counter-propagating superluminal focus ($v = -7.6c\pm20\%$). Extending the pulse duration to $T = 232$ ps slowed the focal spot propagating at $v/c \simeq -0.09\pm1\%$. When the pulse duration was just less than the transit time of the light to propagate across the focal region, the focus was measured to propagate at nearly 50× the speed of light. A positive chirp provides access to a range of forward-propagating subluminal velocities. The focal-spot velocity for a positively chirped laser pulse with a duration of $T = 65$ ps was measured to propagate at $v = 0.20c\pm1\%$.

Figure 151.6 shows snapshots of the longitudinal intensity profiles calculated for three different negative chirp cases. They illustrate propagating backward at the speed of light [Fig. 151.6(a)], propagating instantaneously across the focal volume [Fig. 151.6(b)], and propagating forward faster than the speed of light [Fig. 151.6(c)]. They were calculated by assuming Gaussian optics, $I(z,t)/I_0 = \left[w_0/w(z,t)\right]^2$, where $w_0 \simeq 1/(2G_R)$ is the diffraction-limited spot size and

$$w(z,t) \simeq w_0 \sqrt{1 + \frac{f_0^2}{4Z_R^2}\left[\frac{z}{f_0} + \frac{\lambda_0}{\lambda(\tau)} - 1\right]^2} \qquad (3)$$

is the radius of the flying focus spot. The Rayleigh length for a diffractive lens is given by

$$Z_R \simeq f_0^2\lambda_0 / 4R^2 \simeq 1/4G_R^2\lambda = 52 \ \mu m,$$
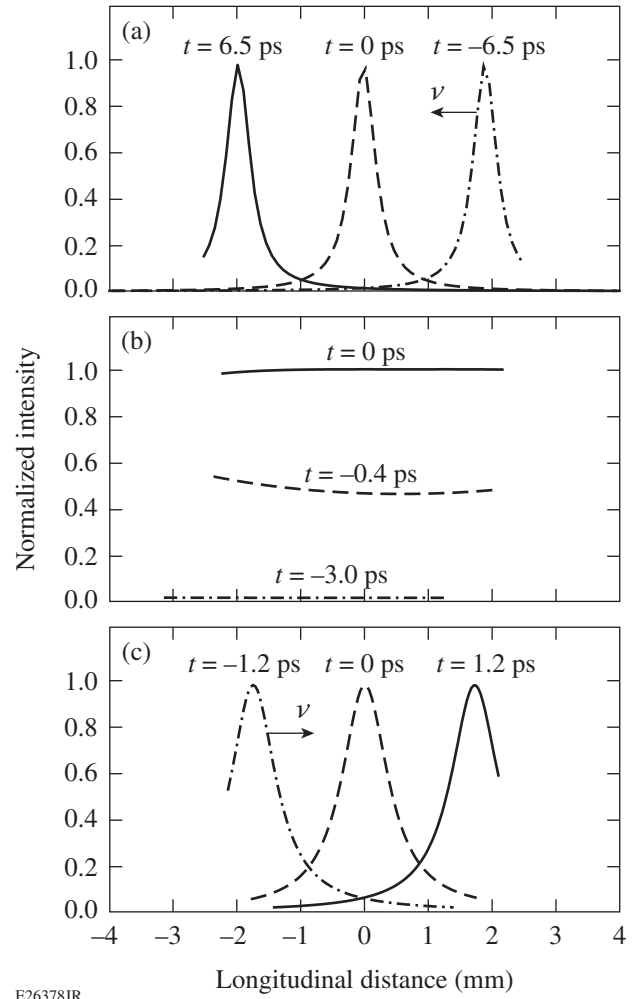


Figure 151.6
The instantaneous longitudinal intensity is plotted for a focus (a) counter-propagating at the speed of light ($T = 2L/c = 29.8$ ps, $\Delta\lambda = -9.2$ nm), (b) propagating at an "infinite" velocity ($T = L/c = 14.9$ ps, $\Delta\lambda = -9.2$ nm) and (c) co-propagating at 5× the speed of light ($T = 0.8 \ L/c = 11.9$ ps, $\Delta\lambda = -9.2$ nm). Snapshots of the intensity profiles at early time (dotted–dashed curves), middle time (dashed curves), and late time (solid curves).

where $G_R$ is the groove density at the radius of the laser beam ($R$). This is a reasonable approach to calculating the intensity profile provided that the pulse duration is much larger than the radial pulse front delay ($T > T_{\text{RPFD}} = 5$ ps).

The intensity of the flying focus across the longitudinal focal region is given by the spectral power, $I(z,t) = P(\lambda)/\pi \left[w(z,t)\right]^2$, which shows that the longitudinal intensity can be controlled by spectrally shaping the laser pulse. In the experiment, 1.6 nm of bandwidth was removed from the middle of a positively chirped spectrum, which demonstrated that the laser did not focus over the central region of the longitudinal focus. The measured laser

focus propagated subluminally ($v/c = 0.16\pm1\%$) over the first ~2 mm and then did not focus again for ~26 ps, at which time the focus reappeared at $z \sim 2.8$ mm and propagated to the end of the longitudinal focal region.

**Applications**

For more-exotic applications, the velocity of the focus can be varied by using a nonlinear chirp and/or a nonlinear chromatic optical system. From Eq. (1), it is evident that the focal velocity could be made to accelerate, decelerate, or oscillate across the longitudinal focal region depending on the design of the nonlinear chirp. An example that demonstrates the impact of the flying focus is a photon accelerator. A photon accelerator frequency upshifts light using rapidly changing density $\left(dn_e/dt\right)$ generated by, for example, an ionization wave. Prior photon accelerator concepts have been limited by phase slippage, where the upshifting laser beam accelerates out of the density gradient.[23] A flying focus using a nonlinear chirp could mitigate this by making the velocity of the ionization wave follow the group velocity of the upshifting beam:

$$\frac{dz}{dt} = v_g(t) = c\sqrt{1 - \omega_p^2/\omega(t)^2}, \qquad (4)$$

where $\omega_p^2 = n_e e^2/m_e \epsilon_0$ and $n_e$ is the maximum electron plasma density. In this case, the photons will be frequency upshifted[27] from an initial frequency $\omega_0'$:

$$\frac{\Delta\omega(t)}{\omega_0'} = \frac{\omega(t) - \omega_0'}{\omega_0'} = \sqrt{1 + \left(\frac{\omega_p}{\omega_0'}\right)^2 \frac{z(t)}{Z_R}} - 1, \qquad (5)$$

where $z(t)$ is the trajectory of the ionization wave (i.e., the trajectory of the flying focus) and $Z_R$ is an approximate width of the ionization wave that was assumed to be equal to the Rayleigh length of the flying focus.

Figure 151.7(a) shows the results from Eq. (5) where photons with an initial group velocity of $v_g = 0.7c$ were accelerated to $v_g = 0.99c$ over 4.5 mm (from $\lambda_0' = 1054$ nm to $\lambda' \simeq 160$ nm at $n_e = 5 \times 10^{20}$ cm$^{-3}$). In a standard photon accelerator design where the ionization wave propagates at a constant velocity given by the initial group velocity of the seed photons, the accelerated photons would be limited to $v_g = 0.9c$ (~550 nm). In this case, the accelerated photons overtake the ionization wave within the first 0.3 mm. The maximum photon energy in a photon accelerator driven by a flying focus is limited by the accelerator length, which is given by the total bandwidth in the laser [$L = f_0(\Delta\lambda/\lambda)$].

Figure 151.7(b) shows the corresponding nonlinear chirp that is required to follow the accelerating trajectory. There are two solutions that both require a negative chirp. The solutions depend on whether the pulse duration of the flying focus is greater than or less than the time it takes for light to transverse the accelerator ($T = L/v_g \simeq 15$ ps). When the pulse duration is
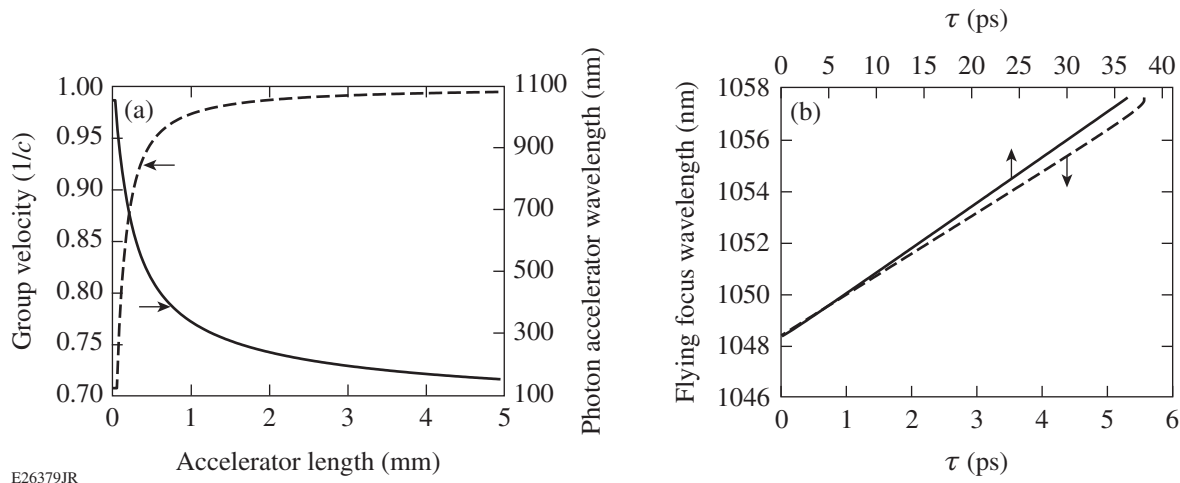


E26379JR

Figure 151.7
(a) The velocity of the accelerating photons (left axis, dashed curve) and their wavelength (right axis, solid curve) are plotted as functions of accelerator length for a system where the ionization wave is produced by an accelerating flying focus. The electron density was assumed to rise from vacuum to $n_e = 5 \times 10^{20}$ cm$^{-3}$ over the Rayleigh length of the flying focus ($Z_R = 0.05$ mm). (b) The nonlinear chirp is required for the flying focus to accelerate in phase with the frequency-shifted photons toward the diffractive lens (bottom axis) and away from the diffractive lens (top axis).

longer than the $L/v_g$, the flying focus will counter-propagate with respect to the flying focus beam; when the pulse duration is shorter than $L/v_g$, the flying focus will co-propagate. This nonlinear chirp accounts for the initial rapidly changing group velocity of the accelerating photons [Fig. 151.7(a)]. Extending the bandwidth to a typical value available in current ultrashort pulse lasers ($\Delta\lambda/\lambda_0 \simeq 200$ nm/1000 nm) lengthens the accelerator to nearly $L \simeq 10$ cm, and the accelerated photons reach a final wavelength of 100 nm, assuming the same conditions for the ionization wave as above. The maximum wavelength shift could be significantly increased by using a density ramp to maintain a constant $\omega_p/\omega'(t)$ as the photons are accelerated.

## Summary

The flying focus provides an avenue for novel control over laser–plasma interactions, removes the need for long-focal-length systems or guiding structures to maintain high intensities over long distances, and decouples the velocity of the focal spot from the group velocity of the light. In addition to photon accelerators, the spatiotemporal control of laser intensity achieved by the flying focus has the potential to change the way plasma devices are optimized and could be applied in many areas of physics. In a laser wakefield accelerator,[28,29] the flying focus could eliminate dephasing by generating a focal spot that moves at a velocity that matches the accelerating electrons. This separation of the accelerator length from the plasma density will provide larger accelerating fields for a given accelerator length and could expand the options for optimizing laser-plasma accelerators. Furthermore, applying the flying focus to a laser-plasma amplifier will allow the ionizing pump laser intensity to propagate at $v = -c$ in order to generate a counter-propagating ionization wave just ahead of the amplifying seed pulse. This will enable one to control the plasma conditions observed by the seed and could be the enabling technology for an efficient laser-plasma amplifier (see the next article, **Raman Amplification with a Flying Focus**).

REFERENCES

1. S. S. Bulanov *et al.*, Phys. Rev. Lett. **105**, 220407 (2010).

2. C. Pellegrini, Eur. Phys. J. H **37**, 659 (2012).

3. C. Joshi and T. C. Katsouleas, Phys. Today **56**, 47 (2003).

4. S. Corde *et al.*, Nature **524**, 442 (2015).

5. C. B. Schroeder *et al.*, Phys. Rev. ST Accel. Beams **13**, 101301 (2010).

6. V. Malka *et al.*, Nat. Phys. **4**, 447 (2008).

7. C. G. Durfee and H. M. Milchberg, Phys. Rev. Lett. **71**, 2409 (1993).

8. S. Jackel *et al.*, Opt. Lett. **20**, 1086 (1995).

9. F. Dorchies *et al.*, Phys. Rev. Lett. **82**, 4655 (1999).

10. D. J. Spence and S. M. Hooker, Phys. Rev. Lett. **63**, 015401(R) (2000).

11. D. H. Froula, L. Divol, P. Davis, J. P. Palastro, P. Michel, V. Leurent, S. H. Glenzer, B. B. Pollock, and G. Tynan, Plasma Phys. Control. Fusion **51**, 024009 (2009).

12. B. Wattellier *et al.*, Opt. Lett. **27**, 213 (2002).

13. E. E. García-Guerrero *et al.*, Opt. Express **15**, 910 (2007).

14. H. Vincenti and F. Quéré, Phys. Rev. Lett. **108**, 113904 (2012).

15. V. M. Malkin, G. Shvets, and N. J. Fisch, Phys. Rev. Lett. **82**, 4448 (1999).

16. J. Ren *et al.*, Nat. Phys. **3**, 732 (2007).

17. R. M. G. M. Trines *et al.*, Nat. Phys. **7**, 87 (2011).

18. G. Vieux *et al.*, Sci. Rep. **7**, 2399 (2017).

19. T. Tajima and J. M. Dawson, Phys. Rev. Lett. **43**, 267 (1979).

20. C. Joshi *et al.*, Nature **311**, 525 (1984).

21. R. Bingham, Nature **394**, 617 (1998).

22. S. M. Hooker, Nat. Photonics **7**, 775 (2013).

23. S. C. Wilks, J. M. Dawson, and W. M. Mori, Phys. Rev. Lett. **61**, 337 (1988).

24. A. Butler *et al.*, Phys. Rev. Lett. **91**, 205001 (2003).

25. J. J. Rocca *et al.*, Phys. Rev. Lett. **73**, 2192 (1994); **75**, 1236(E) (1995).

26. V. Bagnoud, I. A. Begishev, M. J. Guardalben, J. Puth, and J. D. Zuegel, Opt. Lett. **30**, 1843 (2005).

27. J. T. Mendonça, *Theory of Photon Acceleration*, Series in Plasma Physics (Institute of Physics Publishing, Bristol, England, 2000).

28. C. G. R. Geddes *et al.*, Nature **431**, 538 (2004).

29. S. Steinke *et al.*, Nature **530**, 190 (2016).